Performance Analysis of the Capacitively Coupled Radio Frequency Thruster

IEPC-2019-467

Presented at the 36th International Electric Propulsion Conference
University of Vienna • Vienna, Austria
September 15-20, 2019

Arsad Quraishi[1] and Igal Kronhaus[2]
Faculty of Aerospace Engineering
Technion-Israel Institute of Technology, Haifa, 3200003, Israel

Kristof Holste[3] and Peter J. Klar[4]
Institute of Experimental Physics I, Heinrich-Buff-Ring 16, 35392 Giessen, Germany

A miniature capacitively coupled radio-frequency thruster with a capillary tube (C^3RFT) is being developed and tested at the Technion and Giessen University. The thruster utilizes a non-symmetric electrode arrangement and a dedicated radio-frequency generator. The small diameter of the dielectric tube allows operation of the device in very low flow rates, < 8 SCCM in Ar. The ion content in the plume of the C^3RFT was measured using a parallel plate analyzer. It is found that the contribution of ions to the thrust in negligible. The measured thrust time response and wall temperature of 450 C confirm an electrothermal mechanism of thrust generation. At constant input power, the thrust is shown to increase linearly with the flow rate. At an input power of 11 W and a flow rate of 16 SCCM, the thrust nearly doubles compared to the cold flow case, for a total thrust of 350 μN. C^3RFT specific impulse is ≈ 75 s in Ar.

Nomenclature

C^3RFT	=	Capillary Capacitively Coupled Radio Frequency Thruster
IEDF	=	Ion Energy Distribution Function
RFG	=	Radio-Frequency Generator
T	=	Thrust
T_e	=	Electron Temperature
Vrf	=	Time Dependent Voltage
ε_i	=	Ion-kinetic energy

I. Introduction

In the last two decades there is a significant effort by the space community to develop inexpensive miniaturized satellite platforms. Particular attention is given to formation flying missions, where multiple miniaturized satellites are to replace a single large spacecraft [1]. To sustain the formation over the mission period, each individual spacecraft requires a propulsion capability. Many missions are planned around nanosatellites < 20 kg of the CubeSat class [2-3]. Currently, most nanosats are equipped with cold gas thrusters due to their simplicity. However, due to its very low specific impulse, a cold gas propulsion system can take as much as 1/3 of the nanosatellite volume [4].

[1] PhD Student, Aerospace Plasma Laboratory, arsad-qu@campus.technion.ac.il
[2] Head, Aerospace Plasma Laboratory, kronhaus@technion.ac.il
[3] Professor, Institute of Experimental Physics, kristof.holste@exp1.physik.uni-giessen.de
[4] Professor, Institute of Experimental Physics, peter.j.klar@exp1.physik.uni-giessen.de

For low thrust missions such as formation establishment and keeping, electric thrusters are preferred over cold gas thrusters due to their much higher specific impulse. However, the available power for propulsion on a nanosatellite is very limited in the range of 2 - 20 W [5]. Space proven electric propulsion systems such as Hall thrusters and ion thrusters are designed for larger spacecraft and show a significant decrease in performance when scaled to such low power levels [6].

One promising technology for nanosatellite propulsion is the capacitively coupled radio-frequency thruster (CCRFT). In CCRFT, a capacitively coupled radio-frequency discharge is generated inside a dielectric tube operated typically at inlet pressures 1 - 20 torr. The gas is heated inside the tube and accelerated kinetically. Therefore, CCRFT is an electrothermal thruster operating at very low input power. One well studied example is the pocket rocket [7]. This design utilizes a central power electrode placed around a tube with diameter of 2.1 mm and length of 18 mm. A small version is the "mini pocket rocket" which has a tube diameter of 1.6 mm with the same length. Both devices are used at relatively high flow rates of 100 SCCM and 60 SCCM respectively.

In this paper, we study a CCRFT operating at low flow rates, < 20 SCCM of argon, an operational regime that is important for lower thrust applications. Section II describes the design consideration of the capillary capacitively coupled radio-frequency thruster (C^3RFT). Section III presents the experimental setup, and Section IV includes results and discussions.

II. Capillary CCRF Thruster Design

The C^3RFT concept is shown schematically in the Fig. 1. Gas (usually argon) is fed into a dielectric tube with a small diameter (capillary). Two metallic rings are fitted to the tube: a "front" electrode that surrounds the capillary near the exit, and a "back" electrode with direct contact to the capillary's inlet. Energized by rf power, a discharge is ignited between the electrodes. The gas flow is heated by the discharge plasma and ejected from the open end. As the rf frequency is high enough, typically in the 1 - 20 MHz range, electrons are able to follow the alternating electric field whereas ions respond only to time averaged electric fields.

If the electrodes have significantly different surface areas, strong time averaged sheaths are created. Such asymmetric electrode configuration causes the sheath-potential-drop near the smaller surface electrode to increase from $V_s \sim 0.4V_{rf}$ to $V_s \sim 0.8V_{rf}$ [8]. The respective ion kinetic energy gain through a collisionless sheath is given by:

$$\varepsilon_i = V_s + 0.5T_e \quad (1)$$

where T_e is the electron temperature. In addition to the strong potential drop near the electrode, a dc bias will form between the electrodes [8]:

$$V_{bias} = -(\bar{V}_a - \bar{V}_b) \quad (2)$$

where V_a and V_b are driven and grounded electrode voltage amplitude, respectively. In the example shown in Fig. 1 the driven electrode is the front electrode with the smaller surface area. Therefore, $V_a > V_b$ and the driven electrode will be negative with respect to the ground. In this case a time averaged axial electric field is formed directed downstream. For a back driven electrode the reverse will occur.

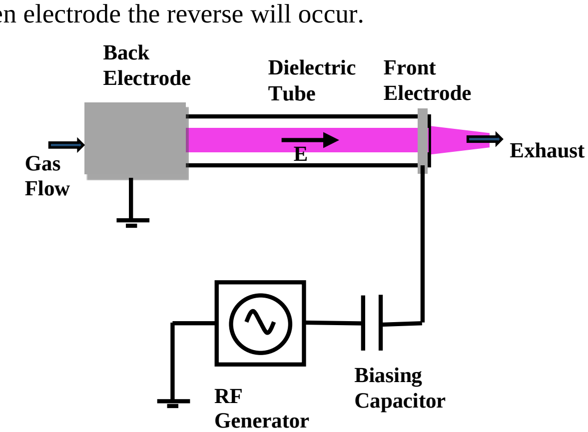

Figure 1. Schematic of the C^3RFT with a front driven electrode.

A. Thruster prototype and cold flow simulation model

A prototype C^3RFT was designed and manufactured in the Aerospace Plasma Laboratory (APL), Technion. The thruster design and its various parts are shown in Fig. 2. The inner diameter of the capillary is d = 0.8 mm and inter-electrode length is l = 15 mm. Thrusters with both alumina and quartz tubes were assembled. The front electrode is a copper ring pressed against the outer wall of the capillary tube using screws, attached at a distance of ~ 1 mm from the exit. The back electrode is a molybdenum tube that is brazed to the capillary. The molybdenum tube itself is brazed to a swagelok type gas feed connector. The propellant gas is fed to the thruster by a flexible teflon tube.

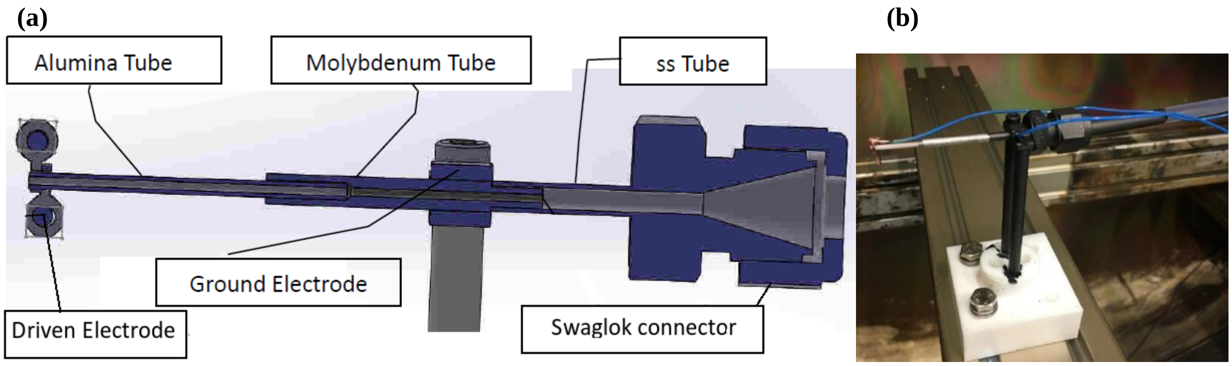

Figure 2. Computer aided design of the C^3RFT, showing the main thruster parts (a) and photograph of the thruster (b).

The cold flow for this C^3RFT configuration was characterized using the commercial computational fluid dynamics (CFD) code CFD-ACE+ [9]. The 2D axisymmetric simulation domain is shown in Fig. 3. The domain represents the top half cross section of the thruster. The mesh is divided into four segments and is refined to be smaller in the regions of interest such as the capillary and near the walls. The discharge capillary volume features a uniform orthogonal rectangular grid consisting of 0.10 × 0.04 mm cells. The molybdenum tube and swagelok connector have the same sized cells. The cells in region downstream of the capillary, which represents vacuum chamber, increase in size with increasing distance downstream. The vacuum outlet boundary has to be included in simulation domain in order to avoid numerical instability and non-physical behavior in the region of interest (capillary).

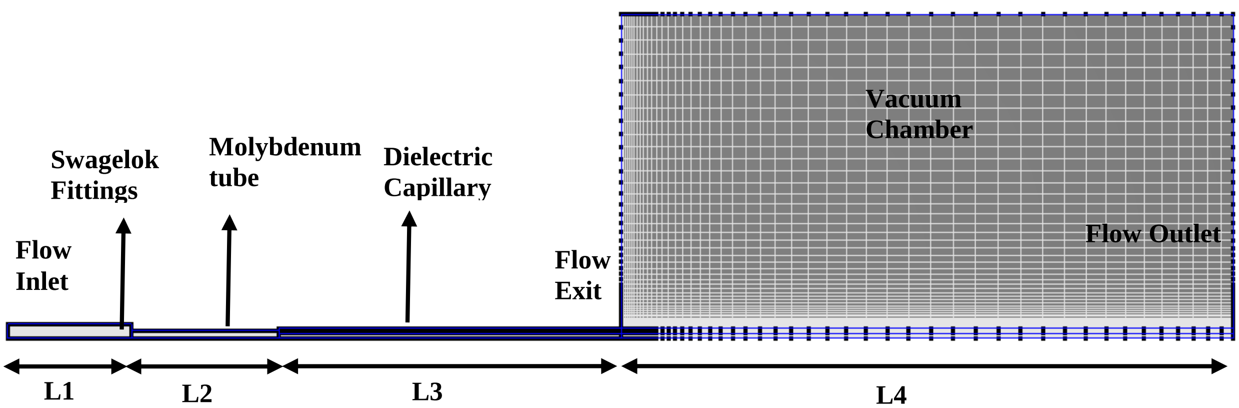

Figure 3. C^3RFT cold flow simulation domain: Swagelok fittings inner radius r = 1.14 mm and length L1 = 10.16 mm, molybdenum tube r =0.6 mm and L2 = 12 mm, dielectric capillary r = 0.4 mm (outer radius 0.8 mm) and L3 = 15 mm length, vacuum chamber r = 50 mm and L4 = 50 mm. The bottom boundary is the axis of symmetry.

The main input for the cold gas simulations is the inlet flow rate of argon and the outlet chamber pressure. The simulation utilizes CFD-ACE+ flow and heat transfer modules, with a transient time step of $\Delta t = 10^{-6}$ s. The temperature of the incoming gas is set at 300 K, and the pressure at the inlet is calculated automatically as the simulation progresses. At the outlet, a fixed pressure is specified, with the value of the experimentally measured vacuum chamber pressure. All the walls are modelled as isothermal with a fixed temperature of 300 K. The solid-fluid interfaces are defined with slip boundary conditions, where the interaction between gas molecules and wall is characterized by tangential momentum accommodation coefficient (TMAC) α_u and thermal accommodation coefficient (TAC) [7, 10] α_T. Here slip boundary conditions using $\alpha_u = 0.9$ and $\alpha_T = 0.9$ were used. The simulation results for 8 SCCM argon flow are presented in Fig. 4. We observe an order of magnitude decrease in gas density inside the capillary. The pressure drops from 10.5 torr at the inlet down to 0.5 torr at the capillary exit. The flow velocity in the capillary, shown in Fig. 4b, reaches sonic velocity at the capillary exit.

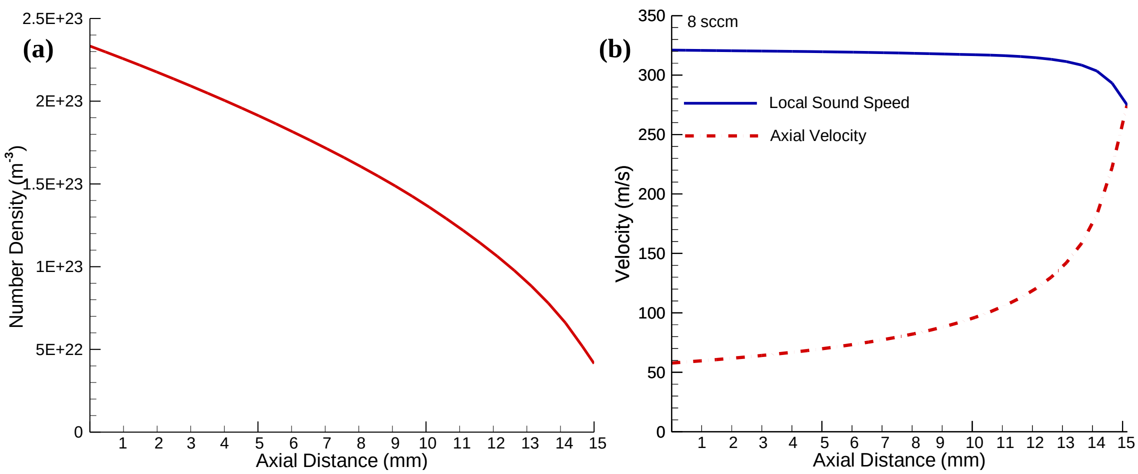

Figure 4. C^{3}RFT cold flow simulation results for 8 SCCM Ar. Results at the axis *r* = 0 mm along the capillary, excluding swagelok and vacuum chamber region: (a) neutral gas number density, axial flow velocity and speed of sound (b). The capillary exit is at 15 mm respectively. 8 SCCM argon flow.

III. Experimental Setup

A. Radio frequency generator

A dedicated radio frequency generator (RFG) was designed and built to power the C^{3}RFT. The RFG was developed by THM Giessen based on their inductive power supply design [11], specifically modified to operate capacitive loads to power the C^{3}RFT. The RFG dimensions are 280 mm x 147 mm x 50 mm. Its operating frequency can be modified between 0.5 - 2 MHz, and the output power 0 - 50 W. The RFG electrical circuit is shown in Fig. 5. The radio frequency generator (RFG) excites a series resonant circuit (oscillator) with a square wave signal. The excitation frequency is automatically controlled to correspond with the resonance frequency of the oscillator. This allows to efficiently generating a sinusoidal signal out of a DC voltage. A series resonant circuit consisting of resonance inductivity Lres and resonance capacity Cres is placed inside of the RFG. If the losses inside the resonant circuit and additional parasitic capacities as well as the thruster capacity are neglected, the resonance frequency f can be estimated by

$$f = \frac{1}{2\pi\sqrt{L_{res}C_{res}}} \tag{3}$$

To change the resonance frequency Cres can be modified. For all the conducted experiments f = 1.8MHz. Ccouple is the biasing capacitor put in series to the thruster; this capacitor is interchangeable and can also be replaced with a short. The amplitude of output voltage Vout can be calculated with

$$V\text{out} \approx V_{\text{DC-link}} \cdot Q \tag{4}$$

where $V_{\text{DC-link}}$ is the DC input voltage and Q is the quality factor of the series resonance circuit.

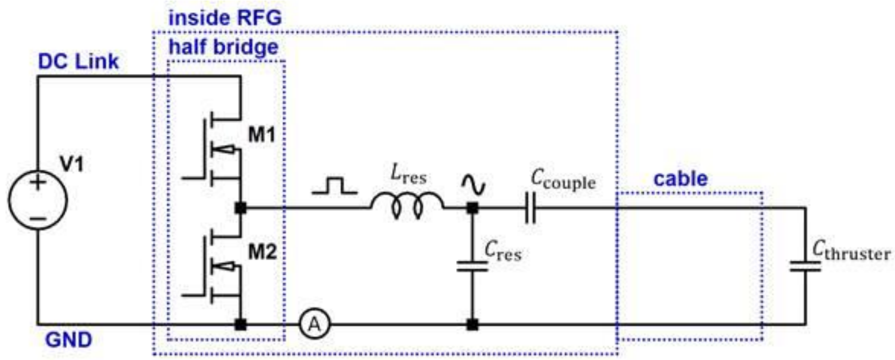

Figure 5. Electrical schematic of the radio frequency generator.

B. Vacuum chamber and setup for thrust measurements
Thrust measurements were conducted in APL's vacuum chamber. The vacuum chamber is a cylinder 1.2 m long and 0.6 m in diameter, equipped with two turbopumps with a combined pumping speed of 1200 l/s for nitrogen, each turbopump is backed by a rotary vane pump. The chamber pressure is measured using a Pirani gauge. During thruster operation at a flow rate of 15 SCCM of argon the chamber pressure was $\approx 3 \times 10^{-4}$ mbar. As shown schematically in Fig. 6, the gas is feed from an external cylinder regulated by 0-100 SCCM flow controller (MKS). The gas line pressure at the vacuum chamber feed-through is measured using a baratron pressure transducer (MKS).

To reduce parasitic capacitance, the C^3RFT and RFG were assembled together inside the vacuum chamber, with the RFG output connected by short wires to the thruster electrodes. The experimental setup in APL's chamber is shown in Fig. 7. The C^3RFT and RFG were mounted on a thrust balance. The torsion balance (FOTEC, Austria) is operated in a displacement mode [12] with measurement resolution of ≈ 1 μN. To avoid torque disturbance, all electric cables powering the thruster were mechanically decoupled using liquid metal contacts. Similarly, the gas line in the chamber is first connected to the thrust balance frame axis, from there a thin teflon tube is used to feed the thruster.

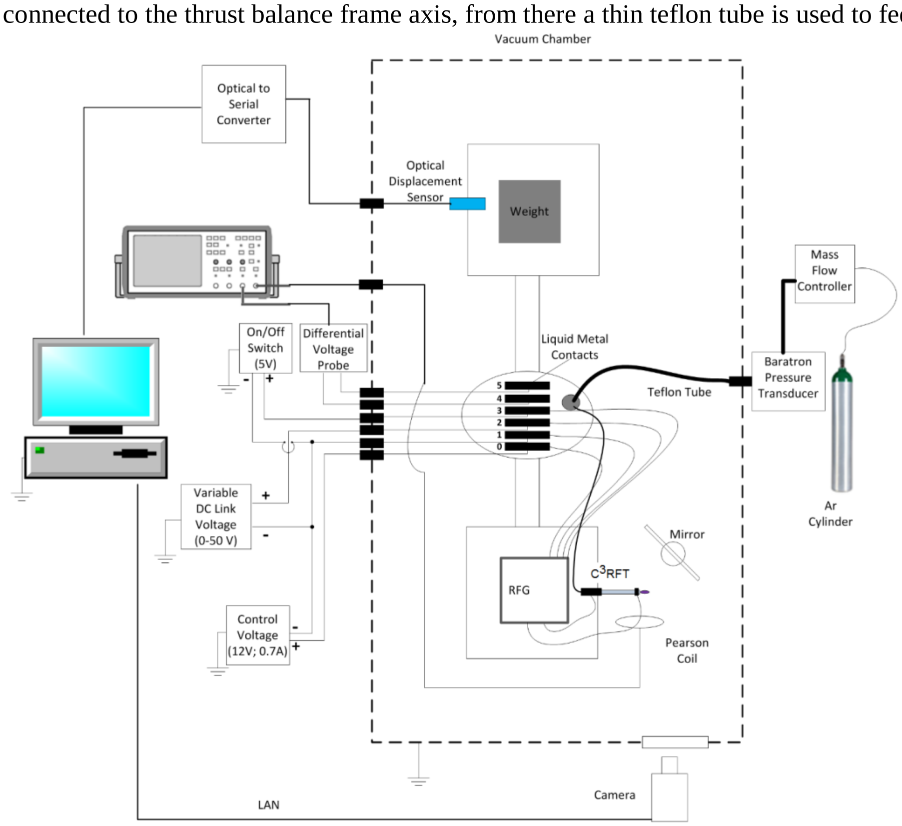

Figure 6. Schematic of the C^3RFT thrust measurement setup in APL.

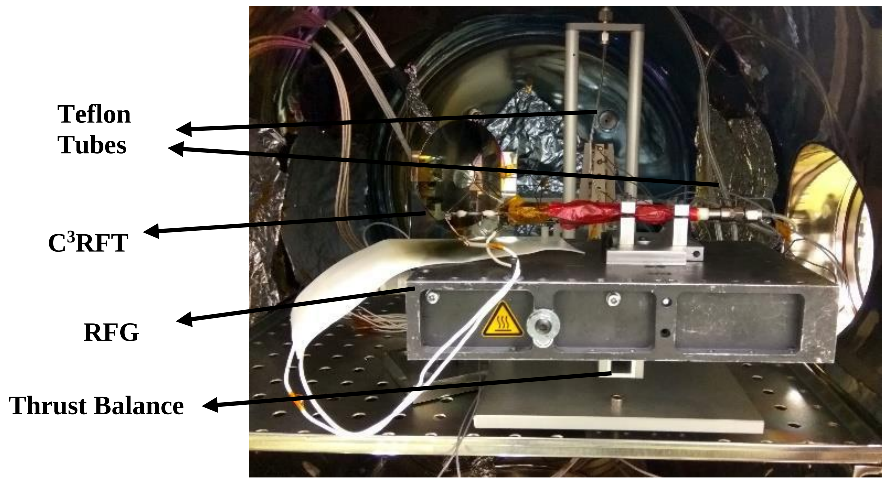

Figure 7. Photograph of the C^{3}RFT thrust measurement setup in APL.

The first set of experiments with C^{3}RFT were used to measure cold flow inlet pressure versus flow rate, and verify the cold flow simulations. For these measurements, two different gas lines were used: 1) the thruster was mounted directly on vacuum chamber wall near the baratron pressure transducer; b) the thruster was connected through the thrust balance teflon tubes. The measured line pressures are shown in Fig. 8. We observe very large pressure losses in flexible Teflon tubes, around ~ 30 torr at 20 SCCM. However, in case of the wall mounted thruster, where only the thruster line pressure is measured, good agreement is obtained with the C^{3}RFT cold flow simulation results.

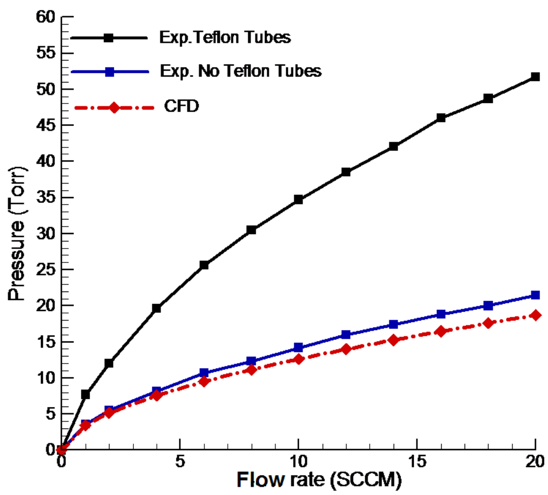

Figure 8. Inlet pressure versus flow rate. Experimental results obtained with and without teflon tubes, simulated (CFD) result obtained using slip boundary conditions α_u=0.9, α_T =0.9.

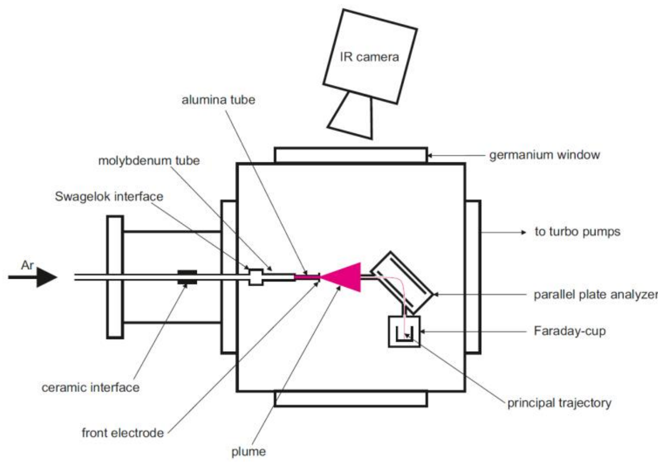

Figure 9. Schematic of ion plume and thermal measurement system.

C. Vacuum chamber and setup for ion energy and thermal measurements

Ion plume measurements were conducted in Giessen University, schematically shown in Fig. 9. The ion energy distribution function (IEDF) of the thruster plume was measured using parallel plate analyzer (PPA) [13]. The PPA collecting diameter was 0.63 cm and placed 18 cm away from thruster exit. An IR camera was positioned outside the chamber looking on the thruster through a germanium window.

IV. Results

A. Electrical measurements results

At first, a reliable ignition procedure for the thruster was characterized, described as follows: first, the mass flow controller was set to the required flow rate and the flow was allowed to stabilize; second, the RFG control voltage was switched on and the DC link voltage was increased gradually until thruster ignition. For a front driven electrode at argon flow rate of 8 SCCM, thruster ignition was obtained at 25 - 35 V and current 0.39 - 0.64 A. The discharge current and voltage characteristics were measured using a Pearson coil and a high voltage differential probe, respectively, on a 5 Gs/s scope. As shown in fig. 10, at nominal operation with DC link of 49 V, the amplitude of rf volatge was found to be +500V/-500V with short (no biasing capacitor, DC current 0.41A) and +500V/-1500V (V_{bias} =-500V DC bias, DC current 0.73A) with biasing capacitor of 1.1nF.

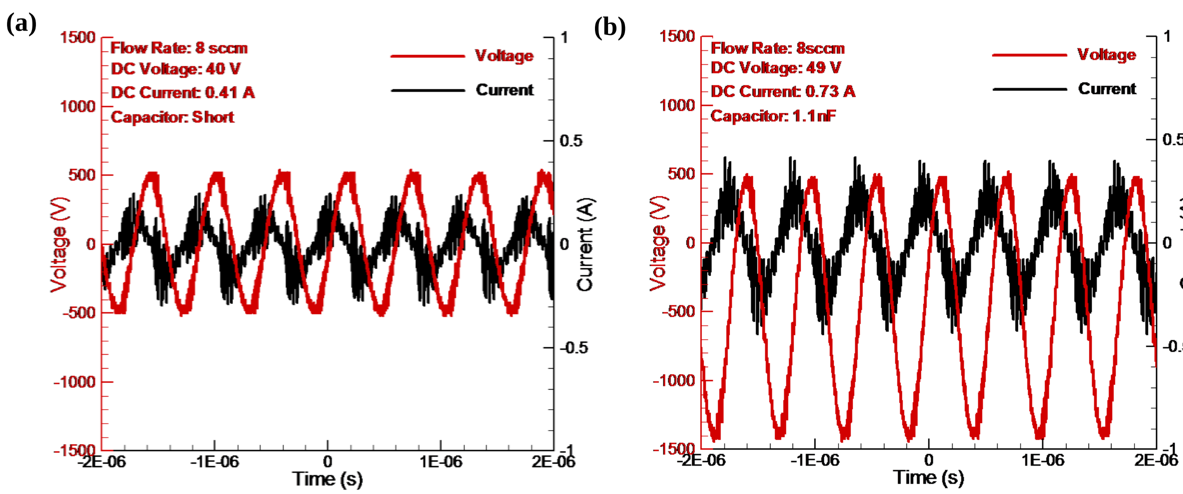

Figure 10. C[3]RFT discharge I-V versus time for RFG and short/no biasing capacitor (a) and with biasing capacitor (b). Front driven electrode at 8 SCCM Ar.

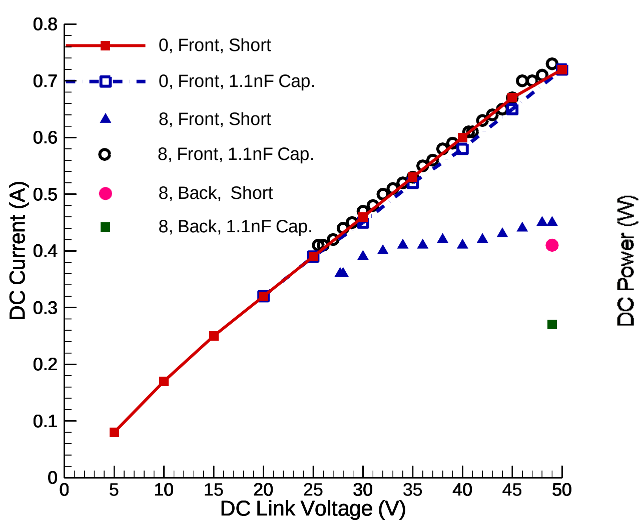

Figure11. RFG DC link current-voltage characteristics. Measured at 0 (no discharge) and 8 SCCM Ar using front and back driven electrode, short and biasing capacitor. Discharge data available only after ignition.

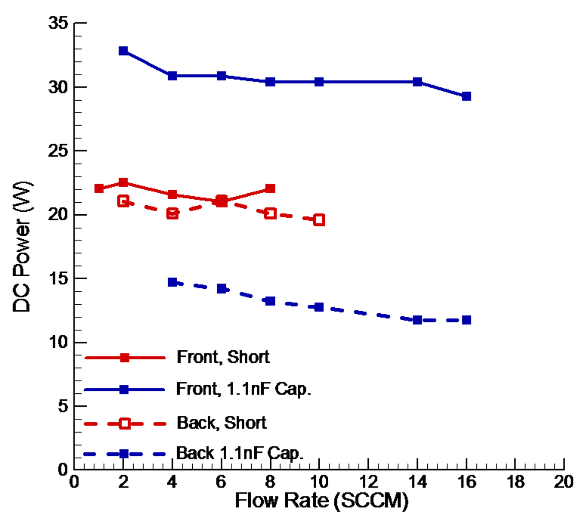

Figure 12. RFG DC link power versus flow rate. DC link voltage of 49V. Using front and back driven electrode, short and biasing capacitor.

Six different cases are shown in Fig. 11. For operation without gas flow (and thus no discharge) the DC link current increases linearly with the voltage. This behavior is attributed to the fact that the electrical load is almost purely capacitive. The same characteristic applies also to an ignited discharge with front driven electrode and biasing capacitor. This is explained by the dominance of the biasing capacitor over the electrical properties of the discharge. For the case of the short/no biasing capacitor we observe a different behavior, where the DC link current is almost constant vs voltage. Here the discharge impedance, in particular the resistive part, influences significantly the DC link I-V. As expected, in this case, using a front or back driven electrode does not change the I-V significantly. The last case is a back driven electrode with biasing capacitor, for which significant reduction in DC link power is observed. In this case power transfer to the discharge increases significantly over the short/no biasing capacitor case and is favorable with regard to total system efficiency (RFG+C^3RFT). The influence of argon gas flow rate on DC link power is shown in Fig. 12. In all cases DC link power is slightly reduced with increasing flow rate.

B. Ion plume and thermal measurement results

The IEDF of the thruster plume was measured in Giessen University using a parallel plate analyzer (PPA) at different flow rates and biasing capacitors. The pressure during operation was kept below 1×10^{-6} mbar. Two results are shown in Fig. 13. For low flow rates (up to 10 SCCM), a double peak structure with amplitude of 0.05 nA is typically measured. As shown in Fig. 14, at certain conditions a luminous plume appears outside the thruster. In such cases the measured IEDF in the plume evolves into a Gaussian like with a single peak at around 180 - 200 eV with amplitude of 0.5 nA. The energy range well corresponds with Eq. (1). However, the low currents suggest that the ions accelerated in the sheaths have negligible contribution to the thrust.

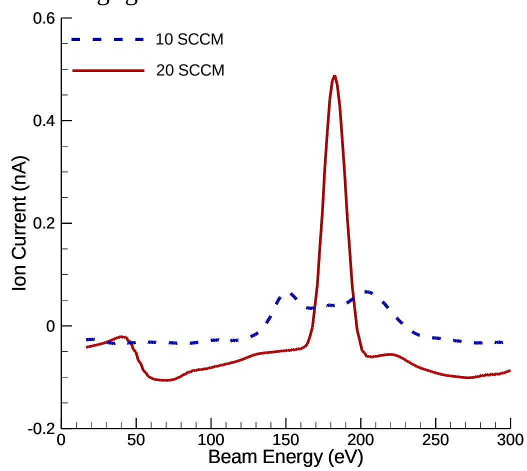

Figure 13. Measured ion energy distribution function in the thruster plume for 10 and 20 SCCM Ar flow rates. Thruster operated with front driven electrode with no biasing capacitor.

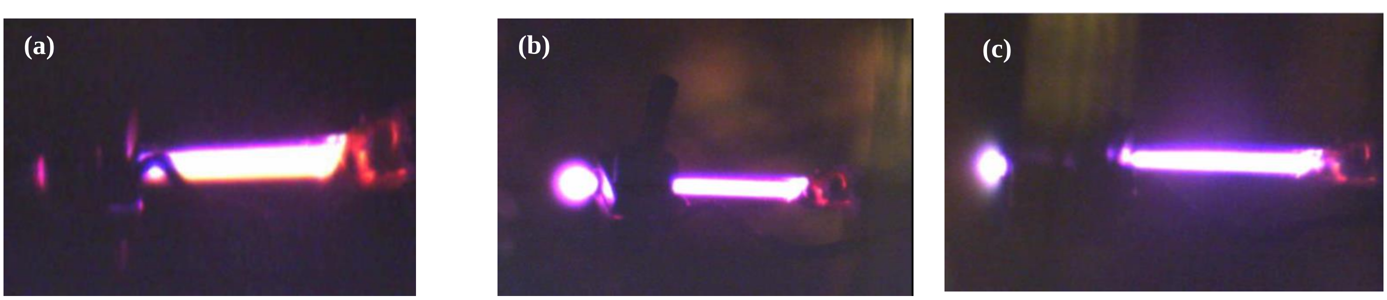

Figure 14. Photographs of a C^3RFT with quartz capillary during operation in vacuum at 8 SCCM Ar: front electrode and biasing capacitor (a), back electrode and biasing capacitor (b), and short/no biasing capacitor (c). The plume in cases (b) and (c) is clearly visible outside the thruster.

Temperature measurements of the C^3RFT capillary tube were conducted using an IR camera at Giessen University. Figure 15 shows an example of measured temperature distribution on the capillary tube. The capillary tube temperature increases monotonically reaching a maximum temperature of 475 °C near the front electrode, then dropping toward the exit of the capillary.

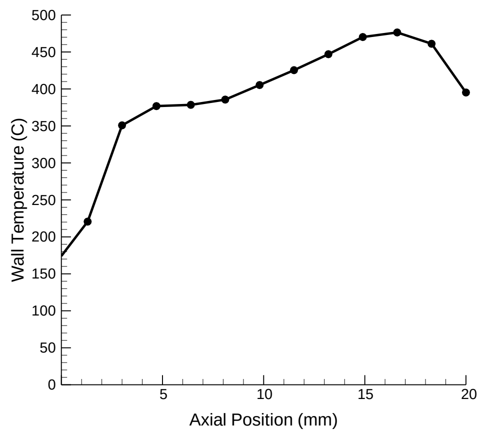

Figure 15. C^3RFT alumina tube temperature versus axial position. Measured during steady state thruster operation for a short/no biasing capacitor case, 8 SCCM Ar and DC link voltage of 49 V.

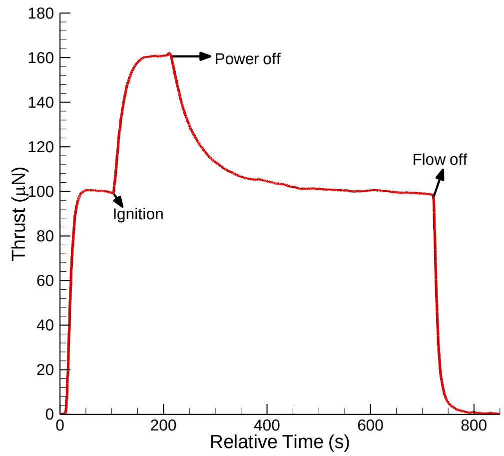

Figure 16. A typical thrust measurement versus time. Front driven electrode with biasing capacitor 8 SCCM Ar and DC link voltage of 49 V.

C. Thrust Measurement Results

Thrust measurement of C^3RFT were performed in APL's 0.25 m^3 vacuum chamber. The installed data equation system integrates the balance deflection response and records a thrust measurement sample every 0.5 s, continuously. Using this relatively high update rate, a time dependent thrust measurement procedure was established, described as follows: 1) the thrust recording is started when the flow is off; 2) the mass flow controller is set to the required flow rate and the flow is allowed to stabilize; 3) the RFG control voltage is switched on and the DC link voltage is quickly set to 49 V; 4) thruster ignition and the thrust balance is allowed to stabilize with full thruster power; 4) the RFG is turned off, the thruster cools down and the thrust balance is allowed to stabilize; 5) the flow is turned off and the balance is allowed to reach reset position again. A sample thrust measurement sequence is shown in Fig. 16. This technique allow perceive thrust measurement and verification of the thrust balance response, in particular it allows to confirm that the thrust balance returns to initial cold flow values and off values. We can also observe that the thruster operates as electrothermal thruster since as the thrust is increasing gradually over time (due to the heat capacitance of the thruster), at much lower rate than the natural thrust balance response time.

Using the above procedure the C^3RFT thrust was characterized for different flow rates, driven electrodes, and capacitor values. Figure 17 shows measured total thrust versus flow rate, with RFG power and without (cold flow), for the cases of front and back driven electrodes with biasing capacitor. As expected, the cold flow results are the same in both cases. When power is applied the different driven electrodes cases produce somewhat different thrust values, but both show considerable thrust enhancement up to 70 % more thrust compared to the cold flow value. As expected, for a constant input power, the thrust is shown to increase linearly with the flow rate. The thruster specific impulse can be calculated by:

$$I_{sp} = \frac{T}{\dot{m}g} \tag{5}$$

where g = 9.81 m/s^2. For the 16 SCCM case the mass flow rate is $\dot{m} \approx 4.75\text{x}10^{-7}$ kg/s, the measured thrust of T ≈ $3.5\text{x}10^{-4}$ N and according to Eq. 5 the I_{sp} ≈ 75 s. This performance level is comparable to the pocket rocket [14] but obtained at lower flow rates and input power.

Figure 18 shows the net thrust added due to RFG power. Here, another case of short/no biasing capacitor is added as well. For flow rates less than 8 SCCM the highest powered thrust is produced by the back driven electrode with biasing capacitor. Above 8 SCCM the front driven electrode produce higher thrust, up to 20 % more than the back electrode at 16 SCCM. However, considering that according to Fig. 12 the power requirement of the back driven electrode is half of the front driven electrode, it is clear that from system efficiency perspective that the back driven electrode is the preferred mode of operation for thruster operation.

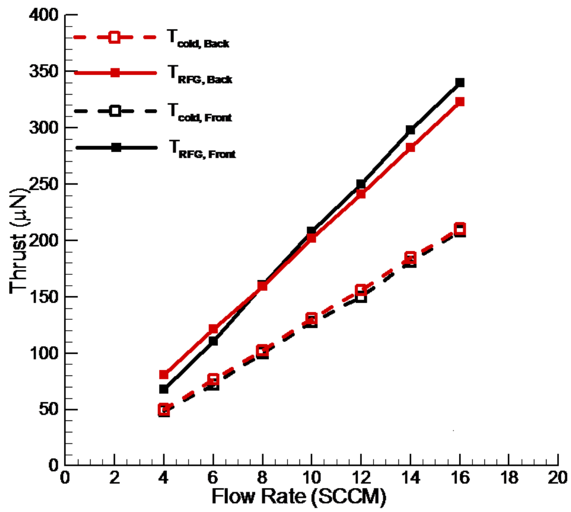

Figure 17. Measured steady state thrust versus Ar flow rate. 2 cold flow cases, 2 cases with discharge using external biasing, one with front driven electrode and another with back driven electrode. DC link voltage 49 V.

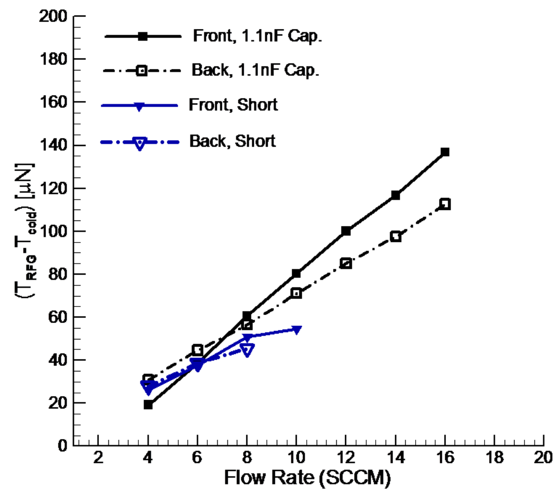

Figure 18. Measured steady state thrust increment due to discharge versus Ar flow rate. 2 cases with and without biasing capacitor, both with front driven electrode and back driven electrode. DC link voltage 49 V.

V.

Conclusion and Future Work

In the present research, the global performance of miniature capacitively coupled RF thruster termed C^3RFT was characterized for low flow rates 4 - 20 SCCM (Ar) using experimental methods and following conclusions can be drawn: 1) Experimental investigation shows significant up to 70 % increase in thrust when RF power is applied with respect to cold flow, producing 350 µN of thrust at rf power of 11 W and argon flow rate of 16 SCCM, specific impulse ≈ 75 s; 2) Ion current measurements were performed on the C^3RFT plume exhaust. The ion current measured was shown to be very small ~ 1 nA, suggesting that the ion content of the plume is insufficient to account for the generated increase in thrust. Thermal measurements show wall temperature of 450 C and gradual accumulation of thrust leading to conclude that the device is operating as an electrothermal thruster.

In the near future, it is planned to characterize the flow and plasma parameters of thruster using optical emission spectroscopy techniques. Fluid plasma simulation of the thruster is also being developed. Future work will also involve improving rf power coupling with the discharge.

Acknowledgments

This work was sponsored by the German-Israeli Foundation for Scientific Research and Development. Grant number I-252-303.2-2015.

References

1. Alfriend, K.T., Vadali S.R., Gurifil P., How J.P., and Breger L.S., *"Spacecraft Formation Flying: Dynamics, Control and Navigation"*, Elsevier Astrodynamics, New York, 2010, Chap. 5.

2. Kronhaus I., Schilling K., Pietza M., and Schein J., *"Simple Orbit and Attitude Control Using Vaccum Arc Thrusters For Pico Satellites" Journal of Spacecrafts and Rockets*, Vol 51, No.6, pp. 2008-2015, 2014

3. "CubeSat Design Specifications (CDS) Rev. 12," The CubeSat Program, California Polytechnic State University, San Luis Obispo, CA, 2009.

4. Sorgenfri M., Stevenson T. and Lightsey G. "Performance Characterisation of a Cold Gas Propulsion System For a Deep Space Cubesat", AAS 17-141

5. Krejci D., and Lozano. P. " Space Propulsion Technology For Small Spacecraft", IEEE, Vol. 106, 2018

6. Daren, Y., Yongjie, D., and Zhi, Z., *"Improvement on the scaling theory of the stationary plasma thruster," Journal of Propulsion and Power,* Vol. 21, No. 1, 2005, pp. 139–143.

7. Ho TS, Charles C. and Boswell R.W. "*A comprehensive Cold Gas Performance Study of the Pocket Rocket Radiofrequency Electrothermal Microthruster*", Frontiers in Physics, 4:55, 2015

8. Lieberman, M. A. and Lichtenberg, A. J., *Principles of Plasma Discharges and Materials Processing*, 2nd ed., Wiley, New Jersey, 2005.

9. https://www.esi-group.com/software-solutions/virtual-environment/cfd-multiphysics/ace-suite/cfd-ace

10. Kogan MN. *Rarefied Gas Dynamics*. New York, NY:Springer (2005)

11. Simon, J. and Probst, U., "Development of a Radio-Frequency Generator for RF Ion Thrusters",International Electric Propulsion Conference, IEPC-2015-289, 2015

12. Seifert B., Reissner A., Buldrini N., and Plesescu F. *"Development and Verification of a µN Thrust Balance for High Voltage Electric Propulsion Systems", 33rd IEPC, The George Washington University, USA, October 6-10, 2013*

13. Green, T. S. and Proca, G. A., "A Parallel Plate Electrostatic Spectrograph", *Rev. Sci. Instrum.*, Vol. 41, pg. 1409, 1970.

14. Charles, C. ,Boswell R. W., Bish, A., Khayms, V., Scholz, E. F., "Direct measurement of axial momentum imparted by an electrothermal radio frequency plasma micro-thruster", *Front Phys*., Vol. 4, pg. 19, 2016.